nature nanotechnology

ARTICLES

https://doi.org/10.1038/s41565-019-0593-9

Two-dimensional mutually synchronized spin Hall nano-oscillator arrays for neuromorphic computing

Mohammad Zahedinejad[1,2,4], Ahmad A. Awad[1,2,4], Shreyas Muralidhar[1,4], Roman Khymyn[1,2], Himanshu Fulara[1,2], Hamid Mazraati[2,3], Mykola Dvornik[1,2] and Johan Åkerman[1,2,3*]

In spin Hall nano-oscillators (SHNOs), pure spin currents drive local regions of magnetic films and nanostructures into auto-oscillating precession. If such regions are placed in close proximity to each other they can interact and may mutually synchronize. Here, we demonstrate robust mutual synchronization of two-dimensional SHNO arrays ranging from 2 × 2 to 8 × 8 nano-constrictions, observed both electrically and using micro-Brillouin light scattering microscopy. On short time scales, where the auto-oscillation linewidth Δf is governed by white noise, the signal quality factor, $Q = f/\Delta f$, increases linearly with the number of mutually synchronized nano-constrictions (N), reaching 170,000 in the largest arrays. We also show that SHNO arrays exposed to two independently tuned microwave frequencies exhibit the same synchronization maps as can be used for neuromorphic vowel recognition. Our demonstrations may hence enable the use of SHNO arrays in two-dimensional oscillator networks for high-quality microwave signal generation and ultra-fast neuromorphic computing.

Interest in bio-inspired oscillatory computing[1–3] is rapidly increasing in an effort to mitigate the inevitable end of Moore's law[4]. Although neuronal activities may seem slow, our brain is the most energy efficient processing device for cognitive tasks thanks to its massively interconnected oscillatory neurons[5]. While recent memristive[6,7], superconducting[8,9], optical[10,11] and micromechanical[12,13] oscillator arrays have been demonstrated, realizing a large physical oscillatory network that meets technical requirements such as room temperature operation, scaling, integration, high speed and low power consumption remains a challenge.

Spin transfer torque nano-oscillators (STNOs) are one of the most promising candidates addressing these requirements[14–16]. Free running STNOs can interact electrically and/or magnetically and mutually synchronize to deliver higher power and more coherent microwave signals with quality factors as high as $Q = 18{,}000$ (ref. [17]). A recent study demonstrated vowel recognition using reservoir computing on four electrically synchronized STNOs[18] achieving a performance comparable to a state-of-the-art complementary metal-oxide-semiconductor (CMOS). However, to process more complicated tasks, large arrays of mutually synchronized oscillators are needed.

Spin Hall nano-osillators[19,20] (SHNOs) have recently emerged as an attractive alternative as they can be fabricated more easily and directly onto silicon substrates[21]. As with STNOs, this makes them compatible with both back and front end of lines in CMOS technology. Their magnetization dynamics is driven by pure spin currents generated by charge currents in a heavy metal layer with a strong spin Hall effect[22–24]. The spin current can exert negative damping on an adjacent ferromagnetic layer and eventually overcome the intrinsic damping, resulting in a steady precession of the magnetization around the effective magnetic field[19].

Nano-constriction SHNOs can be fabricated in chains where they can show mutual synchronization of up to nine individual constrictions[25]. Here, we demonstrate that nano-constriction SHNOs can also be mutually synchronized in two-dimensional (2D) arrays comprising as many as 64 SHNOs. Each oscillator (neuron) in the 2D array interacts with its nearest neighbours via both exchange and dipolar coupling, which can be tuned by both the drive current and the strength and direction of the magnetic field. As expected from theory[26], the signal quality factor of the mutually synchronized state increases linearly with the number of synchronized SHNOs,

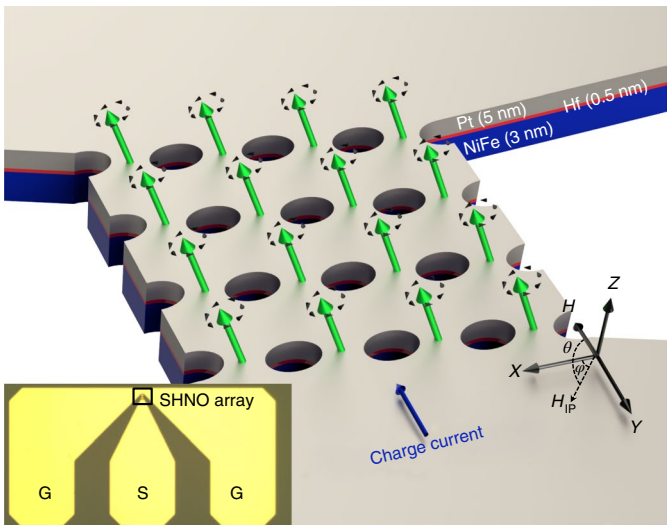

Fig. 1 | Schematic representation of a 4 × 4 SHNO array. The schematic shows the direction of the applied magnetic field (H), its in-plane component (H_{IP}) and the charge current. The green arrows indicate the precessing magnetization of each nano-constriction. The Pt, Hf and NiFe layers are highlighted by grey, red and blue colours with corresponding thicknesses in nm. The inset shows an optical microscopy image of the ground-signal-ground CPW used for electrical measurements.

[1]Physics Department, University of Gothenburg, Gothenburg, Sweden. [2]NanOsc AB, Kista, Sweden. [3]Material and Nanophysics, School of Engineering Sciences, KTH Royal Institute of Technology, Kista, Sweden. [4]These authors contributed equally: Mohammad Zahedinejad, Ahmad A. Awad, Shreyas Muralidhar. *e-mail: johan.akerman@physics.gu.se

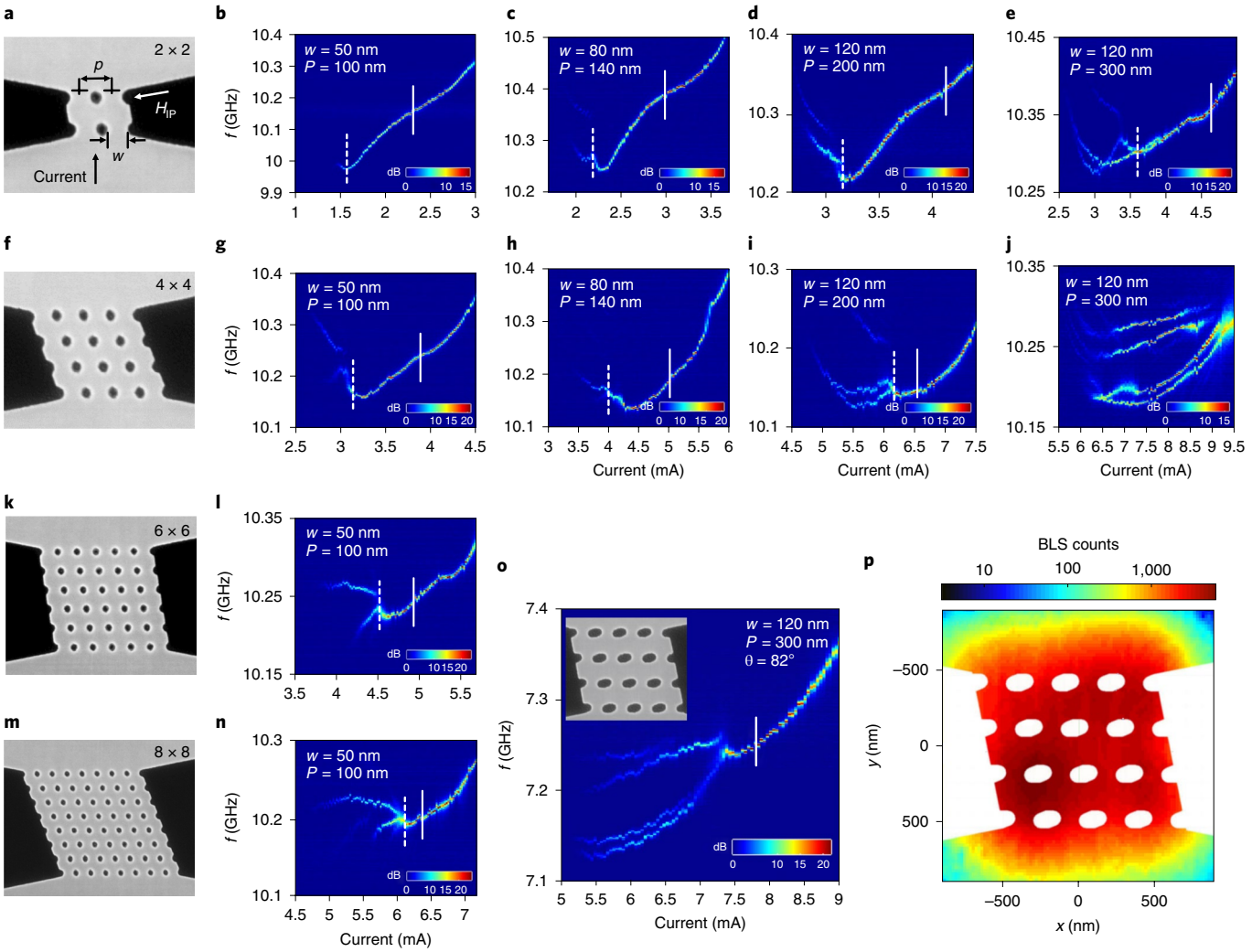

Fig. 2 | PSD and micro-BLS microscopy of SHNO arrays. All data was acquired in a magnetic field of 0.68 T with an out-of-plane angle of 76° and an in-plane angle of 30°. All PSD scale bars are shown in dB over noise floor. **a**, SEM image of a 2×2 SHNO array showing the definition of the width (w) and the pitch (p). The direction of the charge current is shown by a solid black arrow, while the in-plane angle of the applied magnetic field (H_{IP}) is represented by a white solid arrow. **b**–**e**, PSD of four different 2×2 SHNO arrays with different constriction widths (50, 80 and 120 nm) and SHNO centre to centre distance as pitch size (100, 140, 200 and 300 nm). White dashed lines indicate the current at which the SHNOs in the arrays come to a synchronized state. **f**, SEM picture of a 4×4 SHNO array. **g**–**j**, PSD of four different 4×4 arrays having the same width and pitch as the 2×2 arrays in **b**–**e**. Mutual synchronization is only observed in the first three SHNO arrays. **k**,**m**, SEM pictures of a 6×6 (**k**) and an 8×8 (**m**) SHNO array. **l**,**n**, PSD of the 6×6 (**l**) and the 8×8 (**n**) SHNO arrays with the smallest w and p, both showing robust mutual synchronization. **o**, PSD of the same 4×4 array as in **j** with the out-of-plane field angle increased from 76° to 82° to increase the coupling between SHNOs. The inset shows the SEM image of the defined array. **p**, Micro-BLS microscopy image of the 4×4 array in **o** obtained at an operating point of I= 7.6 mA (white dashed line) showing that the entire array contributes to the spin wave excitations in the synchronized state. BLS counts are shown on a logarithmic scale.

reaching Q = 170,000 for 64 SHNOs. We also demonstrate that these arrays lend themselves as-is to neuromorphic computing of the type recently employed for vowel recognition[18]. Adding two microwave currents with different frequencies to the drive current of a 4×4 SHNO array, we demonstrate the emergence of 20 different injection locked states depending on the input combination of the two frequencies.

Schematic of SHNO array and device layout

Figure 1 shows the schematic of an SHNO array with the oscillators illustrated by green arrows precessing around the effective magnetic field (H). The out-of-plane (θ) and in-plane (φ) angles of H are indicated in the coordinate system while the charge current direction is shown by a blue arrow. The Pt, Hf and NiFe layers are shown with their thicknesses in nm and highlighted by blue, red and grey colours, respectively. The ultra-thin Hf layer reduces the spin memory loss at the Pt–NiFe interface[27], which decreases the damping and hence the threshold current. The lower left inset shows the microwave coplanar waveguide (CPW) used for electrical measurements with the location of the SHNO array indicated by a black rectangle (see Methods for sample fabrication details).

Mutual synchronization of SHNO arrays

We fabricated 24 different square SHNO arrays with numbers of nano-constrictions that varied from 2×2 to 10×10, and w and p chosen as (w, p)=(50, 100), (80, 140), (120, 200) and (120, 300), where w defines the constriction width and p stands for pitch (that is, nano-constriction centre to centre distance; all numbers in nanometres). Figure 2a shows a scanning electron microscope (SEM) image of a 2×2 array with the design parameters w and p defined. Figure

2f,k,m in the same column show the corresponding SEM images for 4×4, 6×6 and 8×8 arrays with $(w,p)=(120,200)$ (see Methods). The array has a slight tilt angle to better accommodate the 30° in-plane angle of the applied field, since the auto-oscillating regions extend outwards in a direction perpendicular to this angle.

Figure 2b–e show the power spectral density (PSD) for the four different 2×2 arrays as a function of total drive current through the array. All PSDs show the typical non-monotonic current dependent frequency as the nano-constriction edge mode expands with current[25,28]. All four arrays exhibit mutual synchronization at a synchronization current that increases linearly with w.

Figure 2g–j show the corresponding PSD versus current for the four different 4×4 arrays. While the overall non-monotonic current dependence of the frequency is roughly the same as in the 2×2 arrays, mutual synchronization is now only achieved in the first three arrays. The 4×4 array with 300 nm separation instead shows four distinct individual signals, all with roughly the same linewidth and peak power, indicating partial mutual synchronization. Brillouin light scattering (BLS) scans along the chains and rows of this state reveal that the chains synchronize before the rows (see Extended Data Fig. 1 for details). The coupling strength is hence stronger along the chains than in between chains. The behaviour of the 5×5 array is essentially identical to the 4×4 array: complete synchronization in the first two arrays, partial synchronization at 200 and 300 nm separation (see Supplementary Fig. 1).

Figure 2l and n show the PSD of the 6×6 and 8×8 arrays at the smallest dimensions. At all larger dimensions, neither the 6×6 nor the 8×8 array showed complete mutual synchronization (see Supplementary Fig. 1). Similarly, the 10×10 arrays did not show complete mutual synchronization at any dimension.

The auto-oscillating regions can be expanded by increasing the out-of-plane field angle[28], which should increase the coupling and allow us to synchronize larger arrays. Figure 2o shows a 4×4 array similar to the one in Fig. 2j, but measured at an increased field angle of 82°. The four signals from the individually synchronized chains now merge into a single signal at about 7.3 mA, confirming the important role of the out-of-plane field angle to control the coupling strength. At a separation of 300 nm it then becomes meaningful to explore the spatial profile of the synchronized state using micro-BLS microscopy (~300 nm resolution), as the separation is large enough for variations in the array to be resolved. Figure 2p shows that the entire 4×4 array is energized with a relatively uniform spin wave intensity throughout the array (for a detailed description of the micro-focused BLS measurements, please see ref. [25]).

Linewidth and peak power analysis

In Fig. 3 we summarize the microwave signal properties of all arrays showing complete mutual synchronization. The linewidth plotted in Fig. 3a was chosen as the lowest value observed at certain operating currents (indicated by white solid lines in Fig. 2) in the mutually synchronized regions for ten consecutive measurements for arrays of different sizes. We found this approach yielded consistent values and a consistent trend between arrays, since the frequency showed a tendency to sometimes jump over a much wider range (see Supplementary Figs. 2 and 3). When comparing the individual spectrum analyser measurements, most of them yielded the same narrow linewidth, albeit at different central frequencies, but sometimes the measurement would be artificially broad due to the slower movement of the central frequency. This behaviour suggests two different types of noise: (1) a frequency independent white noise at short time scales, and (2) a $1/f$ - like noise at longer time scales; both noise types are well-established in STNOs[29].

The black dashed line in Fig. 3a is a fit to N^{-1}, which clearly shows how the linewidth in the white noise regime decreases in inverse proportion to the number of mutually synchronized constrictions. This is consistent with the total mode volume, or total energy

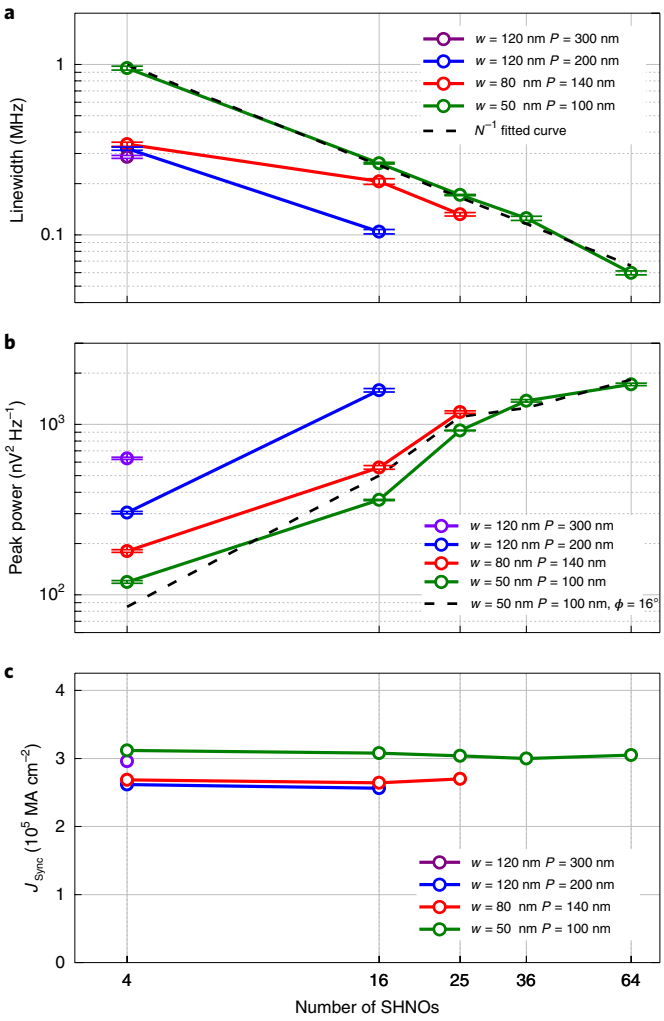

Fig. 3 | Linewidth, peak power and synchronization current density analysis of SHNO arrays. a, Linewidth of arrays of different w and p plotted for those arrays that reach robust synchronization at operating currents indicated by white solid lines in Fig. 2. Black dashed line shows predicted linewidth scaling of $\Delta f \propto N^{-1}$. **b**, Peak power values measured for all synchronized points shown in **a**. Black dashed line indicates the analytical calculation of peak power for arrays with $(w,p)=(50,100)$ considering the phase difference. The error bars (horizontal double lines) in **a** and **b** were obtained from Lorentzian fits to the experimental data. **c**, Synchronization current density for arrays with different (w,p).

of the auto-oscillation state, increasing linearly with N (ref. [26]). As the mode volume scales with w, the linewidth is further reduced in large constrictions. As shown in Supplementary Fig. 4, the $1/f$ noise scales more weakly than N^{-1} and only shows marginal improvement with number of synchronized SHNOs.

Figure 3b shows the synchronization peak power at the same current values (white solid lines in Fig. 2). As the total (integrated) microwave power should increase linearly with N for a mutually synchronized square array[30] we expect the peak power to increase as N^2. While this is observed for small $N=4$–25 for all arrays, the peak power eventually levels off for larger $N=36$–64. This roll off can be reproduced by introducing a small relative phase difference between individual constrictions or between individual chains. While this phase shift is negligible in small arrays, it will add up to a notable phase shift between the constrictions or chains farthest apart in the larger arrays. As the voltages are no longer added exactly in phase, the N^2 scaling will no longer hold. The dashed black line in Fig. 3b

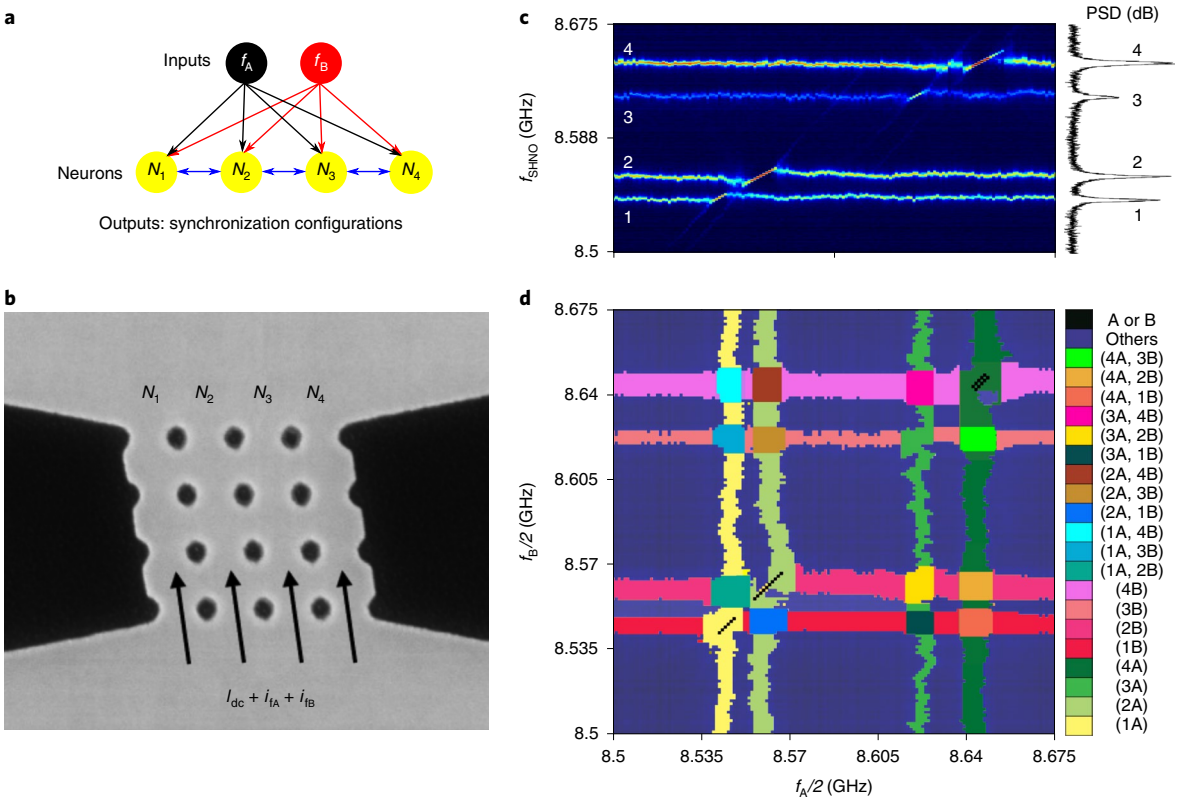

Fig. 4 | Neuromorphic computing with a 4 × 4 SHNO array. a, Schematic of the network where the four neurons (N_{1-4}) interact only with their nearest neighbours while both input current (f_A and f_B) act globally on all four neurons. **b**, SEM picture of the 4 × 4 array where the four synchronized chains act as neurons N_{1-4}, and two microwave currents with frequencies f_A and f_B are added to the drive current. **c**, Injection locking to f_A of each synchronized chain. **d**, synchronization map of the network response when both f_A and f_B are swept individually. A total of 20 different injection locked responses can be observed. Each state is represented by its own colour in the list to the right of the map, where, for example, 1A, 2B indicates that neuron 1 is locked to f_A and neuron 2 is locked to f_B, while the other neurons remain unlocked.

is a calculation of the expected peak power using the measured resistance values for each array and the assumption that there is a chain-to-chain relative phase shift of 16°. The agreement is reasonable and indicates that the peak power would not increase substantially for 10× 10 and larger arrays (see Methods, Estimated PSD section for details).

In Fig. 3c we show how the synchronization current density (J_{Sync}, extracted from white dashed lines in Fig. 2), depends on SHNO array dimensions. J_{Sync} is virtually independent of the number of SHNOs in the array as long as w and p stay the same. For the two arrays with w= 120 nm, we can compare the impact of pitch and conclude that larger separation requires a slightly higher current density for mutual synchronization. However, the overall trend is that J_{Sync} is rather independent on array dimensions at this level of detail.

The low linewidth of ~60 kHz at an operating frequency of ~10 GHz, leads to quality factors as high as $Q = f/\Delta f = 170{,}000$. As the N^{-1} dependence of the linewidth does not show any sign of levelling off for higher N, mutual synchronization of yet larger arrays can be pursued to further improve Q in the white noise regime. The very low white noise linewidth will greatly simplify the design of phase-locked loops[31] to further stabilize the microwave signal, as the phase-locked loop can be optimized for the slower $1/f$ noise still present in the synchronized state.

Prospect for neuromorphic computing

In addition to serving as highly coherent microwave sources, the 2D SHNO arrays can be directly used for neuromorphic computing following an approach implemented using STNO vortex-oscillator chains[18]. As a proof-of-principle we have chosen a 4×4 SHNO array at an operating point where the four individual chains are mutually synchronized internally but do not synchronize with each other (Fig. 4a). The four chains hence serve as the four neurons, N_{1-4}, which in our case interact in a predominantly nearest-neighbour fashion. This is qualitatively different from the chains of vortex-oscillators, where all neurons interacted globally through their shared microwave current[18] Fig. 4c demonstrates that each chain remains in its internally synchronized state when subject to an injected microwave current at about twice its frequency[32] and that each neuron interacts individually with the injected current. Fig. 4d finally shows the characteristic synchronization map[18] of a four-neuron oscillator network subject to two individually swept microwave frequencies f_A and f_B. Each colour represents one of the 20 different injection locked states as indicated to the right of the map. The network can hence distinguish and categorize 20 different input combinations of f_A and f_B.

Using synchronized chains as our neurons, instead of single constrictions, provides both higher coherence and higher output power, which simplifies the identification of the different synchronized states. It also demonstrates that mutual synchronization within chains remains robust under external perturbations necessary for computing, which is an example of the versatility and robustness of the nano-constriction SHNOs. For completeness we point out that we could also generate 20-state synchronization maps using four nano-constrictions in a 2 × 2 array, albeit with less signal quality (not shown).

To train our network, we need a way to tune their individual frequencies. While one could imagine a layout that would allow for individual current tuning of different nano-constrictions or chains, this becomes increasingly complex for larger networks. A more useful approach would be direct voltage control of the magnetic properties in the nano-constriction region, such as magnetic anisotropy and/or damping[33,34], which could tune the SHNO frequency and possibly also turn them on or off at will. Particularly intriguing is the possibility of incorporating a non-volatile element in the voltage control of the magnitude and even sign of the spin orbit torque, as has been recently shown[35,36], to allow for local storage of synaptic weights at each nano-constriction.

A wide range of recently suggested neuromorphic computing approaches are based on large 2D oscillator network with local tuning. Vertex colouring of graphs, which represents a class of combinatorial problems that are non-deterministic polynomial-time hard, can be addressed with oscillator networks[37]. Pattern matching using arrays of multilevel oscillator neurons has been suggested[38,39]. Auto-associative memory based on networks of STNOs and mechanical oscillators has been studied[12,40,41]. Oscillator networks with nearest-neighbour coupling instead of global coupling show particular potential for image segmentation and edge detection[42,43], and can also be used as Ising machines for solving combinatorial optimization problems[44]. The characteristic scale of image segmentation, which determines whether fine or coarse grain details should be clustered together, is further governed by the general nearest-neighbour coupling strength. As we can control this coupling both by the current and/or the external field, image segmentation at variable length scales should be possible using a single 2D SHNO network with voltage-controlled frequencies.

In comparison to one-dimensional STNO chains[18], 2D SHNO arrays have a number of important merits for neuromorphic computing. To perform classification or segmentation of bigger data sets, one must scale up the network as the maximum number of distinguishable classes or segments depend on the number of sufficiently interacting oscillators to provide a useful mix of partially synchronized states. Our SHNO arrays offer a proper scaling path, currently accommodating 100 partially synchronized SHNOs taking up an area of less than 1 μm^2; further down-scaling, using already demonstrated 20 nm SHNOs[45], will bring that number below 0.2 μm^2. The time required to reach a particular synchronized state is expected to scale inversely with the product of the operating frequency and the coupling strength. SHNO operation has been demonstrated at 24 GHz and the mutual locking range is of the order of 1 GHz (refs. [21,25]), both being about two orders of magnitude higher than the corresponding numbers for vortex STNOs[18,46]. The direct optical access may also enable optical inputs to the network.

To truly benefit from these improved characteristics, it will be important to increase the output power by other means than synchronization. The best STNO output power has been demonstrated using magnetic tunnel junctions (MTJs)[47]. MTJ based SHNO arrays should be possible to fabricate using for example W/CoFeB based tri-layers[21], where a W/CoFeB/MgO/CoFeB stack could define an MTJ on top of the auto-oscillating constriction region. By using MTJs over only part of a synchronized array, one may also circumvent the build up of a large phase shift between distant parts of the array.

Conclusion

In conclusion, we have fabricated 2D SHNO arrays with up to $N = 100$ nano-constrictions and demonstrated robust mutual synchronization in arrays with up to $N = 64$ constrictions. We find that the white noise linewidth scales inversely with the number of mutually synchronized constrictions and can reach below 60 kHz at frequencies of about 10 GHz, reaching Q values of 170,000. The $1/f$ noise is only marginally improved. We have also demonstrated how these 2D arrays can produce the type of synchronization maps recently used in neuromorphic computing. Our demonstration will enable the use of SHNO arrays in 2D nano-oscillator networks for high-quality microwave signal generation and neuromorphic computing on very large data sets.

Online content

Any methods, additional references, Nature Research reporting summaries, source data, extended data, supplementary information, acknowledgements, peer review information; details of author contributions and competing interests; and statements of data and code availability are available at https://doi.org/10.1038/s41565-019-0593-9.

Received: 24 January 2019; Accepted: 8 November 2019;
Published online: 23 December 2019

References

1. Grollier, J., Querlioz, D. & Stiles, M. D. Spintronic nanodevices for bioinspired computing. *Proc. IEEE* **104**, 2024–2039 (2016).
2. Pufall, M. R. et al. Physical implementation of coherently coupled oscillator networks. *IEEE J. Expl. Solid-State Comput. Dev. Circ.* **1**, 76–84 (2015).
3. Locatelli, N., Cros, V. & Grollier, J. Spin-torque building blocks. *Nat. Mater.* **13**, 11–20 (2014).
4. Xu, X. et al. Scaling for edge inference of deep neural networks. *Nat. Electron.* **1**, 216–222 (2018).
5. Buzsaki, G. *Rhythms of the Brain* (Oxford Univ. Press, 2006).
6. Kumar, S., Strachan, J. P. & Williams, R. S. Chaotic dynamics in nanoscale NBO 2 Mott memristors for analogue computing. *Nature* **548**, 318–321 (2017).
7. Ignatov, M., Ziegler, M., Hansen, M. & Kohlstedt, H. Memristive stochastic plasticity enables mimicking of neural synchrony: memristive circuit emulates an optical illusion. *Sci. Adv.* **3**, e1700849 (2017).
8. Segall, K. et al. Synchronization dynamics on the picosecond time scale in coupled Josephson junction neurons. *Phys. Rev. E.* **95**, 032220 (2017).
9. Galin, M. A. et al. Synchronization of large Josephson-junction arrays by traveling electromagnetic waves. *Phys. Rev. Appl.* **9**, 054032 (2018).
10. Inagaki, T. et al. A coherent Ising machine for 2000-node optimization problems. *Science* **354**, 603–606 (2016).
11. McMahon, P. L. et al. A fully programmable 100-spin coherent Ising machine with all-to-all connections. *Science* **354**, 614–617 (2016).
12. Fang, Y., Yashin, V. V., Levitan, S. P. & Balazs, A. C. Pattern recognition with 'materials that compute'. *Sc. Adv.* **2**, e1601114 (2016).
13. Shim, S.-B., Imboden, M. & Mohanty, P. Synchronized oscillation in coupled nanomechanical oscillators. *Science* **316**, 95–99 (2007).
14. Csaba, G. & Porod, W. Computational study of spin-torque oscillator interactions for non-Boolean computing applications. *IEEE Trans. Magnet.* **49**, 4447–4451 (2013).
15. Yogendra, K., Fan, D., Jung, B. & Roy, K. Magnetic pattern recognition using injection-locked spin-torque nano-oscillators. *IEEE Trans. Electron Dev.* **63**, 1674–1680 (2016).
16. Chen, T. et al. Spin-torque and spin-Hall nano-oscillators. *Proc. IEEE* **104**, 1919–1945 (2016).
17. Rippard, W. H., Pufall, M. R., Kaka, S., Silva, T. J. & Russek, S. E. Current-driven microwave dynamics in magnetic point contacts as a function of applied field angle. *Phys. Rev. B.* **70**, 100406 (2004).
18. Romera, M. et al. Vowel recognition with four coupled spin-torque nano-oscillators. *Nature* **563**, 230–234 (2018).
19. Demidov, V. E. et al. Magnetic nano-oscillator driven by pure spin current. *Nat. Mater.* **11**, 1028–1031 (2012).
20. Ranjbar, M. CoFeB-based spin Hall nano-oscillators. *IEEE Magnet. Lett.* **5**, 1–4 (2014).
21. Zahedinejad, M. et al. CMOS compatible w/cofeb/mgo spin Hall nano-oscillators with wide frequency tunability. *Appl. Phys. Lett.* **112**, 132404 (2018).
22. Demidov, V. E. et al. Magnetic nano-oscillator driven by pure spin current. *Nat. Mater.* **11**, 1028–1031 (2012).
23. Demidov, V. E., Urazhdin, S., Zholud, A., Sadovnikov, A. V. & Demokritov, S. O. Nanoconstriction-based spin-Hall nano-oscillator. *Appl. Phys. Lett.* **105**, 172410 (2014).
24. Fulara, H. et al. Spin-orbit torque–driven propagating spin waves. *Sci. Adv.* **5**, eaax8467 (2019).
25. Awad, A. et al. Long-range mutual synchronization of spin Hall nano-oscillators. *Nat. Phys.* **13**, 292–299 (2017).
26. Kim, J.-V., Tiberkevich, V. & Slavin, A. Generation linewidth of an auto-oscillator with a nonlinear frequency shift: spin-torque nano-oscillator. *Phys. Rev. Lett.* **100**, 1–4 (2008).

27. Mazraati, H., Zahedinejad, M. & Åkerman, J. Improving the magnetodynamical properties of Nife/Pt bilayers through HF dusting. *Appl. Phys. Lett.* **113**, 092401 (2018).
28. Dvornik, M., Awad, A. A. & Åkerman, J. Origin of magnetization auto-oscillations in constriction-based spin Hall nano-oscillators. *Phys. Rev. Appl.* **9**, 014017 (2018).
29. Keller, M. W., Pufall, M. R., Rippard, W. H. & Silva, T. J. Nonwhite frequency noise in spin torque oscillators and its effect on spectral linewidth. *Phys. Rev. B.* **82**, 054416 (2010).
30. Georges, B., Grollier, J., Cros, V. & Fert, A. Impact of the electrical connection of spin transfer nano-oscillators on their synchronization: an analytical study. *Appl. Phys. Lett.* **92**, 232504 (2008).
31. Tamaru, S., Kubota, H., Yakushiji, K., Yuasa, S. & Fukushima, A. Extremely coherent microwave emission from spin torque oscillator stabilized by phase locked loop. *Sci. Rep.* **5**, 18134 (2015).
32. Demidov, V. et al. Synchronization of spin Hall nano-oscillators to external microwave signals. *Nat. Commun.* **5**, 3179 (2014).
33. Matsukura, F., Tokura, Y. & Ohno, H. Control of magnetism by electric fields. *Nat. Nanotech.* **10**, 209–220 (2015).
34. Liu, R., Chen, L., Urazhdin, S. & Du, Y. et al. Controlling the spectral characteristics of a spin-current auto-oscillator with an electric field. *Phys. Rev. App.* **8**, 021001 (2017).
35. Mishra, R. et al. Electric-field control of spin accumulation direction for spin-orbit torques. *Nat. Commun.* **10**, 248 (2019).
36. Mishra, R., Kumar, D. & Yang, H. Oxygen-migration-based spintronic device emulating a biological synapse. *Phys. Rev. Appl.* **11**, 054065 (2019).
37. Parihar, A., Shukla, N., Jerry, M., Datta, S. & Raychowdhury, A. Vertex coloring of graphs via phase dynamics of coupled oscillatory networks. *Sci. Rep.* **7**, 911 (2017).
38. Velichko, A., Belyaev, M. & Boriskov, P. A model of an oscillatory neural network with multilevel neurons for pattern recognition and computing. *Electronics* **8**, 75 (2019).
39. Zhang, T., Haider, M., Massoud, Y. & Alexander, J. An oscillatory neural network based local processing unit for pattern recognition applications. *Electronics* **8**, 64 (2019).
40. Kumar, A. & Mohanty, P. Autoassociative memory and pattern recognition in micromechanical oscillator network. *Sci. Rep.* **7**, 411 (2017).
41. Nikonov, D. E. et al. Coupled-oscillator associative memory array operation for pattern recognition. *IEEE J. Expl. Solid-State Comput. Dev. Circ.* **1**, 85–93 (2015).
42. Fang, Y., Yashin, V. V., Jennings, B. B., Chiarulli, D. M. & Levitan, S. P. A simplified phase model for simulation of oscillator-based computing systems. *ACM J. Emerg. Tech. Comput. Syst.* **13**, 14 (2017).
43. Novikov, A. & Benderskaya, E. in *International Conference on Parallel Computing Technologies* (ed Malyshki, V.) 210–221 (Springer, 2015).
44. Wang, T., Wu, L. & Roychowdhury, J. New computational results and hardware prototypes for oscillator-based Ising machines. In *Proc. 56th Annual Design Automation Conference 2019* 239 (ACM, 2019).
45. Dürrenfeld, P., Awad, A. A., Houshang, A., Dumas, R. K. & Åkerman, J. A 20 nm spin Hall nano-oscillator. *Nanoscale* **9**, 1285–1291 (2017).
46. Lebrun, R. et al. Mutual synchronization of spin torque nano-oscillators through a long-range and tunable electrical coupling scheme. *Nat. Commun.* **8**, 15825 (2017).
47. Tsunegi, S. et al. Scaling up electrically synchronized spin torque oscillator networks. *Sci. Rep.* **8**, 13475 (2018).

Methods

Sample fabrication. To fabricate SHNO arrays, an ultra-high vacuum magnetron sputtering machine was used to deposit a tri-layer of $Ni_{80}Fe_{20}$ (3 nm)/Hf (0.5 nm)/Pt (5 nm) at room temperature on a high resistivity silicon substrate (10 kΩ cm^{-1}). The native oxide layer on the substrate was removed by plasma cleaning before the deposition process. The Ar pressure during deposition was kept at 3 mTorr. The sample was then covered by 37 nm of hydrogen silsesquioxane (HSQ) electron beam resist and SHNO arrays were written in HSQ by a Raith EBPG 5200 electron beam lithography machine operating at 100 kV. The patterns were then transferred to the tri-layer by ion beam etching process at a 30° ion incident angle with respect to the film normal to minimize sidewall re-depositions. SHNO arrays were defined with different constriction widths (w=50, 80 and 120 nm) and SHNO centre to centre distance as pitch size (P=100, 140, 200 and 300 nm). Because the curvature of the nano-constriction is an elliptical arc, for the larger P values the shape of the holes defined in the tri-layer is more elliptical. However, for smaller P values, the holes look more circular. The curvatures of the nano-constrictions in all arrays with different ws and ps are identical. To define the top CPW contact for d.c. and microwave measurements, optical lithography was performed followed by HSQ removal only at contact areas in diluted buffered hydrofluoric acid. Finally, a 1 μm thick layer of Cu (980 nm)/Pt (20 nm) was deposited, and CPWs were obtained after resist removal by the lift-off process.

Microwave characterization. We used a custom-built probe station where the stage can rotate the sample holder between the poles of an electromagnet to apply an out-of-plane magnetic field to the sample. The in-plane and out-of-plane angles of the sample were fixed at 30° and 76°, respectively, while the magnetic field was set to $\mu_0 H = 0.68$ T for all measurements. A direct current was applied through the d.c. port of a bias-T to excited auto-oscillation in SHNO array while the emitted microwave signal from the array was picked up by the high frequency port of bias-T and was sent to a low noise amplifier (LNA) in the 4–10 GHz range before it was recorded by a high frequency spectrum analyser. The recorded spectra were then corrected to correspond to the power emitted by the device, taking into account the amplifier gain, the losses from the radio frequency components and cables, and the impedance mismatch between the device and the 50 Ω measurement line and load. The auto-oscillation linewidth and peak power were extracted by fitting a single symmetric Lorentzian function. To perform the neuromorphic computing demonstration, we used a microwave power combiner connected to a microwave circulator to inject two microwave signals into the SHNO arrays. The injected power for the two signals f_A and f_B was limited to −2 dBm to avoid any damage to the LNA and the spectrum analyser. f_A and f_B were chosen to be close to $2f_{SHNO}$; that is, we injection locked on the second harmonic.

Estimated PSD. We consider the power delivered by the array of $K \times M = N$ oscillators to the load R_l, taking into account the finite resistance of the mesa R_m. For a perfectly synchronized state, without any phase shift between oscillators, the power reads as[30]:

$$P_N = \left[\frac{KMI_{dc}\Delta R_{ac}}{KR_c + M(R_l + R_m)}\right]^2 R_l \quad (1)$$

where M defines the quantity of parallel branches with K serial oscillators in each of them and, thus, for our case $K = M = 2, 4, 5, 6, 8$. $R_l = 50$ Ω is load resistance, $R_m = 200$ Ω is the resistance of the sample outside the array region (mesa); $R_c = 80$ Ω is the resistance of each nano-constriction; I_{dc} is the d.c. current applied to each oscillator and R_{ac} is the alternate resistance created by the magnetization precession through anisotropic magnetoresistance, which we assume as a fitting parameter.

Please note, that the above expression results in the proportionality of the delivered power to the total number of oscillators N for the square arrays, when $K = M$. Since the measured power deviates from such a scaling, we allow for a phase shift ϕ between neighbouring chains. In this case, assuming the Lorentzian shape of the PSD with the linewidth Δf defined by full width at half maximum, one can write the maximum value of the PSD:

$$PSD_{max} = \frac{2}{\pi\Delta f}\left[\frac{KI_{dc}\Delta R_{ac}}{KR_c + M(R_l + R_m)}\sum_{j=0}^{M-1}\cos j\phi\right]^2 R_l^2 \quad (2)$$

which is shown by a dashed line on Fig. 3b with the fitted value $\phi = 16.4°$. Please note, that in the synchronized state the linewidth Δf should be inversely proportional to the total power of auto-oscillators, that is, to the total number N, and does not depend on the phase shift ϕ (ref. [48]).

Data availability

The data that support the plots within this paper and other findings of this study are available from the corresponding author on reasonable request.

Code availability

The MATLAB codes used in this study are available from the corresponding author on reasonable request.

References

48. Wiesenfeld, K., Benz, S. P. & Booi, P. Phase-locked oscillator optimization for arrays of Josephson junctions. *J. Appl. Phys.* **76**, 3835–3846 (1994).

Acknowledgements

This work was partially supported by the European Research Council (ERC) under the European Union's Seventh Framework Programme (FP/2007-2013 ERC Grant no. 307144 'MUSTANG') and Horizon 2020 research and innovation programme (ERC Advanced Grant no. 835068 'TOPSPIN'). This work was also partially supported by the Swedish Research Council (VR) and the Knut and Alice Wallenberg Foundation.

Authors contributions

M.Z. designed and fabricated the devices, and carried out most of the electrical measurements and analysis of their microwave signal properties. A.A.A. and S.M. carried out all BLS measurements and analysis as well as the neuromorphic demonstration. R.K. and M.D. assisted with theoretical support and analysis. H.F. and H.M. assisted with microwave measurements and analysis. J.Å. coordinated and supervised the work. All authors contributed to the data analysis and co-wrote the manuscript.

Competing interests

The authors declare no competing interests.

Additional information

Extended data is available for this paper at https://doi.org/10.1038/s41565-019-0593-9.

Supplementary information is available for this paper at https://doi.org/10.1038/s41565-019-0593-9.

Correspondence and requests for materials should be addressed to J.Å.

Peer review information *Nature Nanotechnology* thanks Kyung-Jin Lee and the other, anonymous, reviewer(s) for their contribution to the peer review of this work.

Reprints and permissions information is available at www.nature.com/reprints.

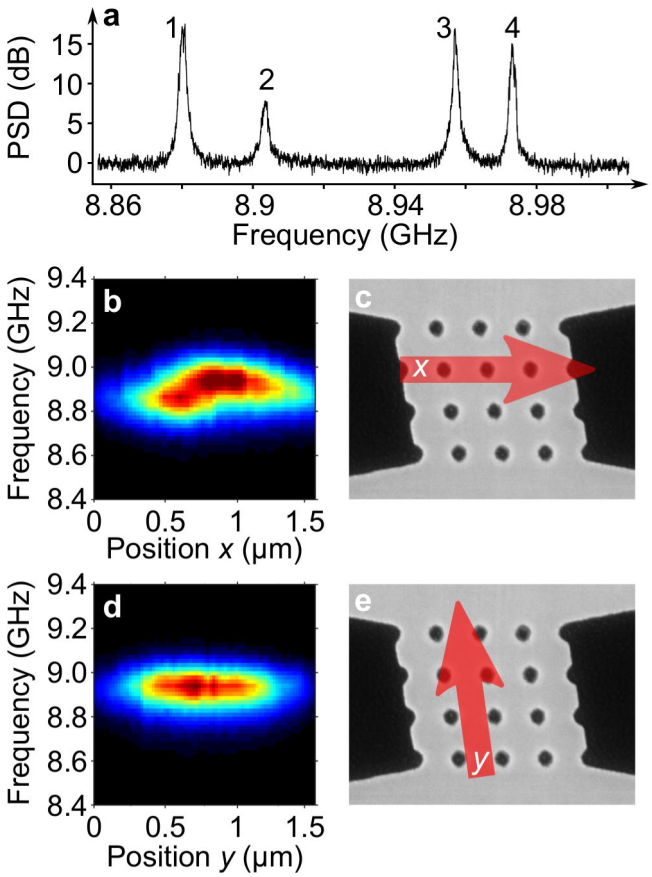

Extended Data Fig. 1 | Linear micro-Brillouin Light Scattering microscopy profile along a row and a chain in a 4x4 SHNO array of 120 nm wide nano-constrictions separated by 300 nm. (**a**) The power spectral density at $H = 0.6$ T and $I = 7$ mA, where four strong and stable modes are observed in the spectrum. To determine whether the partial synchronization is related to chains or rows we carried out Brillouin Light Scattering (BLS) microscopy line scans along both chains and rows. (**b**) A plot of the BLS counts and the frequency measured as a function of position along the red arrow shown in (**c**) reveals that the 4 oscillators are not operating at the same frequency. In contrast, (**d**) a similar scan along a chain as highlighted in (**e**) shows a constant BLS peak frequency independent of the position along the y-axis. This serves as conclusive proof that the oscillators first synchronise along each chain followed by the synchronization of all the chains together.